minerals

MDPI

Article

Surface Spectroscopy of Pyrite Obtained during Grinding and Its Magnetisation

Martín Reyes [1,*], Guadalupe Herrera [1], Ramiro Escudero [2], Francisco Patiño [3], Iván A. Reyes [4], Mizraim Flores [5], Elia G. Palacios [6], Julio Juárez [1] and Francisco Barrientos [1]

1 Área Académica de Ciencias de la Tierra y Materiales, Universidad Autónoma del Estado de Hidalgo, Mineral de la Reforma 42186, Mexico
2 Instituto de Investigaciones Metalúrgicas, Universidad Michoacana de San Nicolás de Hidalgo, Morelia 58030, Mexico
3 Ingeniería en Energía, Universidad Politécnica Metropolitana de Hidalgo, Tolcayuca 43860, Mexico
4 Instituto de Metalurgia, Universidad Autónoma de San Luis Potosí, San Luis Potosí 78210, Mexico
5 Área de Electromecánica Industrial, Universidad Tecnológica de Tulancingo, Tulancingo 43642, Mexico
6 Escuela Superior de Ingeniería Química e Industrias Extractivas, Instituto Politécnico Nacional, Ciudad de Mexico 07738, Mexico
* Correspondence: mreyes@uaeh.edu.mx

Abstract: During grinding with forged steel media, sulphides such as pyrite undergo surface changes due to the occurrence of oxidation–reduction reactions, which affect its depression during the concentration process. For this reason, in this work, the surface modification of pyrite during grinding was studied; FTIR, ICP-OES, XRD and SEM-EDS were used for the materials' characterisation. It was found that the pyrite obtained during grinding showed magnetic susceptibility due to the absorption and superficial formation of magnetite Fe_3O_4, Fe–O bonds identified by FTIR at 598 cm^{-1}, and of other species, such as oxy-hydroxy-sulphates at 696 cm^{-1} and goethite α-FeOOH at 875 cm^{-1}. This caused the reversal of the zeta potential magnitude (ζ) from positive to negative at pH 8.3 and 30 min of grinding. The ζ of the pyrite throughout the studied pH ranges was, overall, positive, i.e., +5 mV. However, at pH 10.5 and 15 min of grinding, the ζ turned negative. This was associated with the formation of Fe–CO_3 (−2) bonds in the siderite, which were identified with the absorption bands corresponding to 756, 1448 and 1493 cm^{-1}.

Keywords: infrared; pyrite; magnetite; grinding; goethite; siderite

Citation: Reyes, M.; Herrera, G.; Escudero, R.; Patiño, F.; Reyes, I.A.; Flores, M.; Palacios, E.G.; Juárez, J.; Barrientos, F. Surface Spectroscopy of Pyrite Obtained during Grinding and Its Magnetisation. *Minerals* **2022**, *12*, 1444. https://doi.org/10.3390/min12111444

Academic Editor: Gianfranco Ulian

Received: 27 September 2022
Accepted: 11 November 2022
Published: 15 November 2022

1. Introduction

The oxidation of pyrite during grinding with steel media is a relevant and constant subject of study [1], as it is considered a common impurity in deposits of base metal sulphide ores [2]. On the other hand, due to the fact of its mineralogical association with gold, it is also considered a valuable mineral [3]. In the first case, it is desirable to depress it and, thus, avoid its floating together with valuable minerals [4]; in the second case, it must be separated from precious metals (i.e., gold and silver) so they can be recovered [3].

The depression of sulphides is attributed to the surface adsorption of worn-out products and the oxidation of iron from the steel in grinding media [5], although pyrite in mineral concentrates is rather abundant and can amount to more than 25% [6]. The negative impact of grinding on the surface contamination of sulphides by iron species, such as hydroxides, oxy-hydroxides and sulphates, formed by galvanic reactions derived from multiple contacts between the iron in the grinding media and the semiconductor sulphides, has been documented [7].

Pyrite has a rest potential against a standard hydrogen electrode (SHE) of +0.66 V measured at pH 4 [3,8], while that of mild steel measured in distilled water exposed to the atmosphere is −0.374 V [3,7]. The difference between these values is considerable

and produces a sharp effect on galvanic interactions during grinding due to the greater galvanic current amplitude [3]. In other words, electrons released in the oxidation of iron to ferrous iron, taking place on the steel surface and acting as an anode, are transferred onto the cathodic mineral, i.e., pyrite. Therefore, precipitated iron species are indiscriminately adsorbed into its surface [8], leading to extensive corrosion of iron from the grinding medium, possessing a lower rest potential than pyrite, whilst the corrosion of pyrite decreases, being more cathodic [9–12]. The importance of studying the surface behaviour of pyrite during grinding lies on its abundance in the ore deposits of base metal sulphides (Cu, Pb and Zn), as it is an undesirable phase that contaminates mineral concentrates.

Grinding is the last stage in mineral comminution before the concentration process. Industrial mills have an internal polymer layer that protects the shell; forged steel balls of different diameters are used with the aim of reducing the particle size to release the valuable species from the gangue and to optimize separation during the flotation stage. Nowadays, it is known that both reactions and physical interactions occur between the grinding media and sulphides during grinding [13]. For instance, iron (II) disulphide (FeS_2) (i.e., pyrite) is the most reactive sulphide [14]. Due to the fact of its composition of ionic Fe–S bonds and covalent S–S bonds [15], it is the most common metallic impurity in mineral deposits [14]. Studying its behaviour during grinding is of great importance to optimize its separation from valuable minerals. Previous works have studied the changes pyrite undergoes during grinding [1].

The wide occurrence of pyrite, the variety of processes in which it is present, and the economic impact it represents, makes it a mineral whose study is of great relevance, especially regarding the surface modification it undergoes during grinding, leading to surface reactions. Thus, determining the speciation and surface reaction mechanisms of pyrite during grinding is crucial.

Iron oxides, hydroxides, and oxy-hydroxides are abundant materials in nature as well as in the field of mineral processing, such as the grinding process. The most common and thermodynamically stable species are hematite Fe_2O_3, goethite α-FeOOH and magnetite Fe_3O_4. In a smaller proportion and considered stable metaphases, maghemite γ-Fe_2O_3, lepidocrocite γ-FeOOH, akaganeite β-FeOOH, feroxyhyte δ-FeOOH and ferrihydrite Fe_5HO_8*$4H_2O$, can be found. Feroxyhyte and the gamma species are ferromagnetic [13–15].

Along with these species, schwertmannite has been reported as an oxy-hydroxy-sulphate of iron present in chemical environments containing iron and sulphates, such as those typical of sulphide mineral grinding pulps [16,17]. The identification of these precipitated solids during pyrite grinding is particularly relevant for understanding the chemical and structural speciation of iron sulphide, as well as its effect on electrokinetic properties.

The surface of pyrite exposed to aqueous environments that contain carbonates has been extensively studied by FTIR [18–21]; multiple absorption bands typical of sulphate ions that form on the surface of pyrite were identified. Despite the relevance of the information, oxide, hydroxide and iron sulphate phases on the surface of pyrite are not distinctly identified, as they are difficult to detect by XRD due to the fact of their faintly crystalline nature as well as their relatively low concentration in the mineral surface. FTIR spectroscopy studies on pyrite oxidation during grinding are scarce, and the existing literature is focused on the spectrum range between 900 and 1500 cm^{-1}.

Despite the large amount of relevant information obtained in these studies on the oxidation products related to pyrite, no detailed information regarding the surface speciation of mineral sulphide particles obtained during grinding is available. Likewise, the state of the chemical coordination between sulphur and iron on the mineral surface and its effect on the electrokinetic properties of pyrite particles, as well as the magnitude and polarity of the surface charge and its reactivity and capability to sorb or desorb anions as a function of the grinding pH, are not thoroughly approached.

In this work, the surface speciation and magnetisation of pyrite obtained during grinding, by determining the chemical nature of the pulp, was carried out. For such purposes, the effect of the grinding pH on the oxidation–reduction potential, concentration of dissolved oxygen, electrokinetic behaviour of the pyrite particles and the electrical conductivity of the mineral pulp were studied. The electrokinetic behaviour was determined through the zeta potential, and the pyrite solids were characterised by ICP-OES, XRD, FTIR and SEM-EDS.

2. Materials and Methods

2.1. Equipment and Reagents

A sample of 6 kg of pyrite from the mining region of Zimapan, Hidalgo, Mexico, were used. The mineral was homogenised, fragmented and stored in sealed plastic containers; a sample of 200 g of the homogenised mineral was used for characterisation purposes. The +0.63–0.8 cm size fraction was used for all of the grinding experiments. The chemical composition of the sample, determined by ICP-OES, is shown in Table 1.

Table 1. Chemical composition of pyrite.

Mineral	**Elemental Composition (% *w*/*w*)**							
	Fe	S	Cu	Pb	Zn	Ca	Na	Si
Pyrite	43.71	54.12	0.138	0.010	0.004	0.003	0.001	0.371

The total percentage (100%) of the elements of the pyrite was not quantified.

For the grinding process, a 6 L steel mill without lining and 6 kg of forged steel grinding media (carbon steel particles; d = 2.54 cm (66.7%) and 1.27 cm (33.3%)) were used. One litre of solution and 400 g of mineral were used for each grinding test, at a 40 RPM mill rate. Solutions of 1M NaOH and 1M H_2SO_4 were used for pH adjustment at alkaline and acidic values, respectively. Deionised water was employed in all the experiments.

2.2. Experimental Procedure

The grinding tests were carried out at different initial pH values (5, 7, 9, 11, 12 and 13), and 0.05 L pulp aliquots (mineral + water) were taken at 5, 15, 30 and 45 min grinding time, immediately resuming the experiment. The chemistry of the pulp (i.e., pH, oxidation–reduction potential (mV), dissolved oxygen concentration DO and electrical conductivity k (μS/cm)) was monitored in all of the pulp samples. Thermo Scientific Orion benchtop pH meters and a Hach conductivity meter were used for the recordings. The oxidation–reduction potential values are expressed as the potential of standard hydrogen electrode *Eh* (pulp potential), thus adding +245 mV to the obtained value [22].

The pulp was filtered (0.45 μm Millipore), and the concentration of the metal iron and sulphur in the grinding solution was analysed by ICP. The dispersion of the pyrite particles in the pulp for each grinding time and pH value was analysed as a function of its zeta potential value (ζ; mV); the obtained solids were examined by XRD, FTIR and SEM-EDS.

A series of grinding experiments, analogous to those carried out with the pyrite but only with the grinding media and the solutions, were also performed. The solutions contained dispersed solids, and the pulp potential values in relation to the SHE were always positive, ranging between +521 and +695 mV SHE. The concentration of dissolved oxygen and pH did not undergo the drastic changes seen in the pyrite grinding experiments. In addition, precipitation tests of the ferric and ferrous iron from their sulphate salts at different concentrations were conducted in order to obtain the ζ values for the Fe (+3) and Fe (+2) precipitates, which are species present during grinding. The precipitated solids were also characterised by XRD and FTIR to determine the formed phases.

The precipitation tests were conducted separately in a wide range of concentrations and pH, using ferric sulphate $Fe_2(SO_4)_3 \cdot nH_2O$ and ferrous sulphate $Fe(SO_4) \cdot 7H_2O$, both analytical grade with 72% and 90% purity, respectively. The following concentrations were employed: 0.09, 0.18, 0.36, 0.72, 1.43 and 2.86 mM Fe (+3) and only 2.86 mM Fe (+2).

For the precipitation of ferric and ferrous iron, 1 L of solution was used for each initial pH value, gradually varying the pH by one unit (1M NaOH) up to 13, keeping the stirring rate constant at 1000 RPM. To simulate the conditions of a real grinding pulp, H_2SO_4 (4.79 mM) was added exclusively in the case of the solutions containing the ferric sulphate salt to have an initial pH of approximately 2.0. For the ferrous sulphate solutions, the pH of the initial dissolution was between 3.7 and 5.2 for the higher and lower initial concentration of Fe (+2), respectively. Once the precipitates sedimented, the solution was decanted, and the solids formed were washed with abundant water prior to characterisation.

2.3. Zeta Potential Measurements

The zeta potential measurements were performed in a Malvern Panalytical (Nanoseries Malvern Inc., Worcestershire, UK) zetasizer. The thickest particles were left to settle, and the supernatant containing the finest particles was transferred into a vertical–rectangular electrophoresis cell to conduct the measurement of the electrophoretic mobility of the mineral at room temperature. Then, using the Smoluchowski equation, the zeta potential (ζ; mV) was calculated. Each test was carried out in triplicate, and the average value is presented.

2.4. FTIR Analysis

The infrared spectra were recorded in a Perkin Elmer Spectrum GX spectrometer (4000–400 cm^{-1}; 2 cm^{-1} resolution). Samples of 0.01 g were mixed with 0.1 g of binder (infrared grade KBr), compressed into pellets (hydraulic press) and immediately analysed. The spectral bands identification was carried out by comparison with a spectral database of iron and sulphur compounds and with absorption bands reported in the literature.

3. Results and Discussion

3.1. Chemistry of the Grinding Pulp

The experimental results obtained from pyrite grinding with steel media show that the studied physicochemical properties of the pulp (i.e., pH, DO, k and oxidation–reduction potential) changed constantly during the whole grinding time. For the tests conducted at an initial pH of 5–9, the potential of the hydrogen ions of the pulp increased gradually after the first five minutes of grinding, as shown in Figure 1a. According to the reaction $O_2 + 2H_2O + 4e^- \rightarrow 4OH^-$, where 1 mol of oxygen produces four moles of hydroxyl ion, this detected increase in the pH was due to the cathodic process, where the decrease in the concentration of dissolved oxygen is caused by galvanic contact (corrosion).

Therefore, a significant decrease in the DO concentration was present since the first minutes of grinding, reaching final values practically equal to zero throughout the studied pH range, as observed in Figure 1b. DO does not participate in the oxidative dissolution, acting only as a receptor of the electrons generated by the oxidation reaction of pyrite [23].

In the tests conducted at initial values of 11–13, the pH decreased as the grinding time elapsed (Figure 1a). This pH decrease in the strongly alkaline media was due to the consumption of OH^- ions, as indicated by the following reaction: $OH^- = Ad_{sorbed} + e^-$, where the highest availability of the hydroxyl ion OH^{-1} produces hydroxylation and a higher surface oxidation of pyrite. Thus, two oxidation reaction mechanisms of pyrite can be clearly distinguished: one in the 5–9 range and another between 11 and 13.

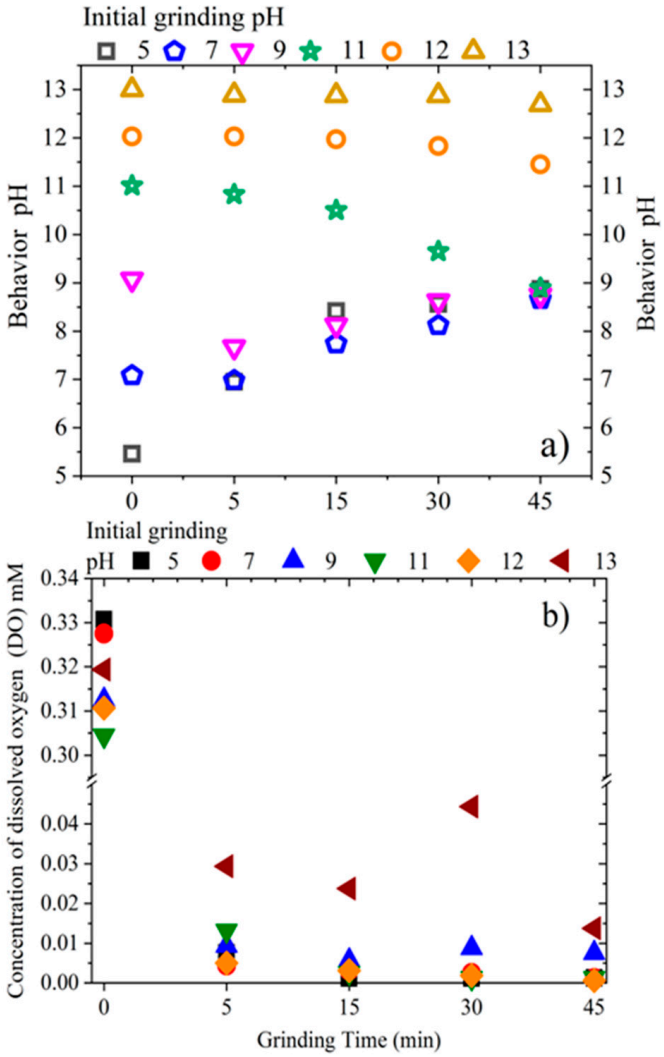

Figure 1. (**a**) pH behaviour as a function of grinding time (initial pH 5–13); (**b**) concentration of dissolved oxygen vs. grinding time (pH 5–13).

As to the electrical conductivity (*k*) of the pulp (graph not included in this work) when the pH was between 11 and 13, it decreased as the grinding time passed. This was due to the elevated consumption of OH^- ions adsorbed into the pyrite surface, where superficial iron oxides or hydroxides are formed. This decrease in *k* was also attributed to the formation of aqueous compounds that did not have a charge, such as hydrated sodium sulphate $Na_2SO_4 \times 10H_2O$ ΔG° −871.379 Kcal/mol, which was identified by the *Eh*–pH diagrams. The *k* decreased despite the constant increase in the iron and sulphur concentrations analysed by ICP in the solution. Figure 2a,b show the iron and sulphur concentrations in the pulp solution, respectively.

The electrical conductivity (*k*) in the pH range 5–9 increased as the reaction time passed, until reaching values of approximately 216 $\mu S \cdot cm^{-1}$. This was due to the presence of iron and sulphur ions in the solution, produced from the oxidation of pyrite, the mill and the grinding media as well as from the increase in the concentration of OH^{-1} in the solution. The sulphur in the solution was 8, 84 and 157 times higher at an initial pH of 11 for 12, 13 and 45 min of grinding, compared to that found at pH 6, 7 and 9, respectively. It was transformed into its more stable species in aqueous medium (i.e., sulphate), which was neutralised by OH^{-1} ions coming from the cathodic reaction of DO; a similar behaviour has previously been reported [14].

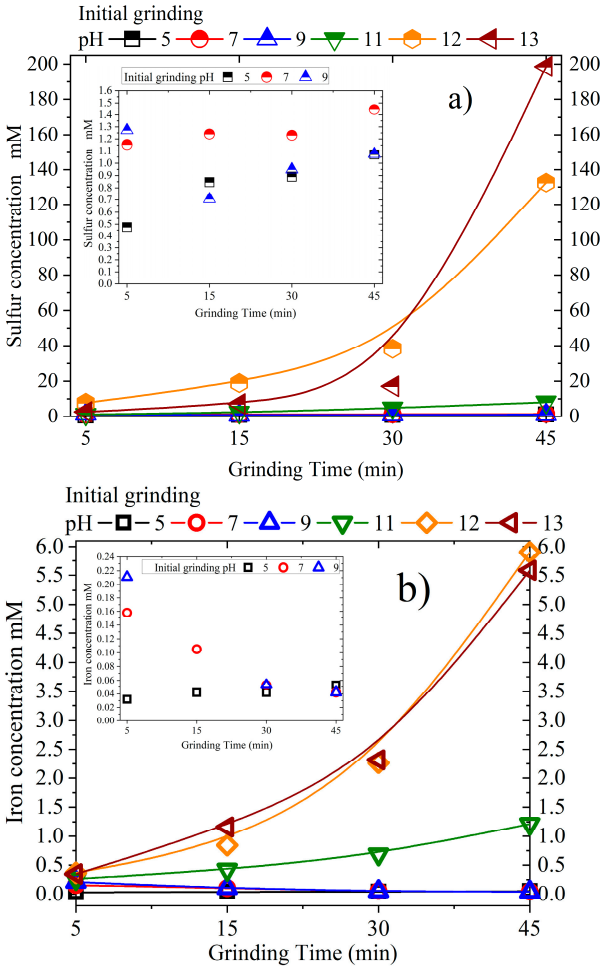

Figure 2. (**a**) Iron concentration (mM) as a function of grinding time (minutes); (**b**) sulphur concentration (mM) as a function of grinding time (minutes).

The slope change detected in both the sulphur and iron concentrations in the solution of the grinding pulp was attributed to the larger surface oxidation of the pyrite, with an increase in the surface area generated during grinding. The lesser concentration of the iron in the solution compared to that of the sulphur was due to the precipitation of iron oxide or hydroxide as a solid species, thus diminishing its concentration in the solution.

Figure 3 shows the *Eh*–pH diagram of the Fe–S–H_2O system at 25 °C, 1 M, where the values of the pulp potential (*Eh*) are also plotted. When the initial pH of the grinding pulp was between 5 and 9, the most thermodynamically stable species were iron oxide-hydroxide (neutral aqueous species) Fe (OH)O(a) and iron III oxyhydroxide precipitated as $FeO^{x}OH$. Further, the type of solid precipitated or formed on the pyrite surface was determined in the IR analysis.

On the other hand, in the initial pH range 11–13, the iron in the aqueous phase transformed into iron III oxide, FeO_2 (−a). We noted that at initial values lower than 9, the pH tended to increase and the pulp potential decreased as the grinding time passed; its magnitude also changed, shifting towards negative potentials. These changes occurred when the grinding time was equal to or longer than 15 min.

The dotted lines in the diagram in Figure 3 represent the zones of thermodynamic stability of the aqueous phases in the Fe–S–H_2O system at 25 °C, 1M. When the initial pH of the pulp was higher than 11, the pulp potential decreased its positive value as the grinding time passed. In addition, the pH decreased when its initial value was 13, and at 45 min, the pulp potential (*Eh*) turned negative. The pulp potential is an indicator of the electron transfer between solid and aqueous species resulting from the oxidation reactions

of pyrite during grinding. In fact, pyrite oxidation with OH^- ions generates $14e^-$ by mol of FeS_2, as indicated by Reaction (1).

$$FeS_2 + 8OH^- = Fe^{2+} + 2SO_4^{2-} + 8H^+ + 14e^- \quad (1)$$

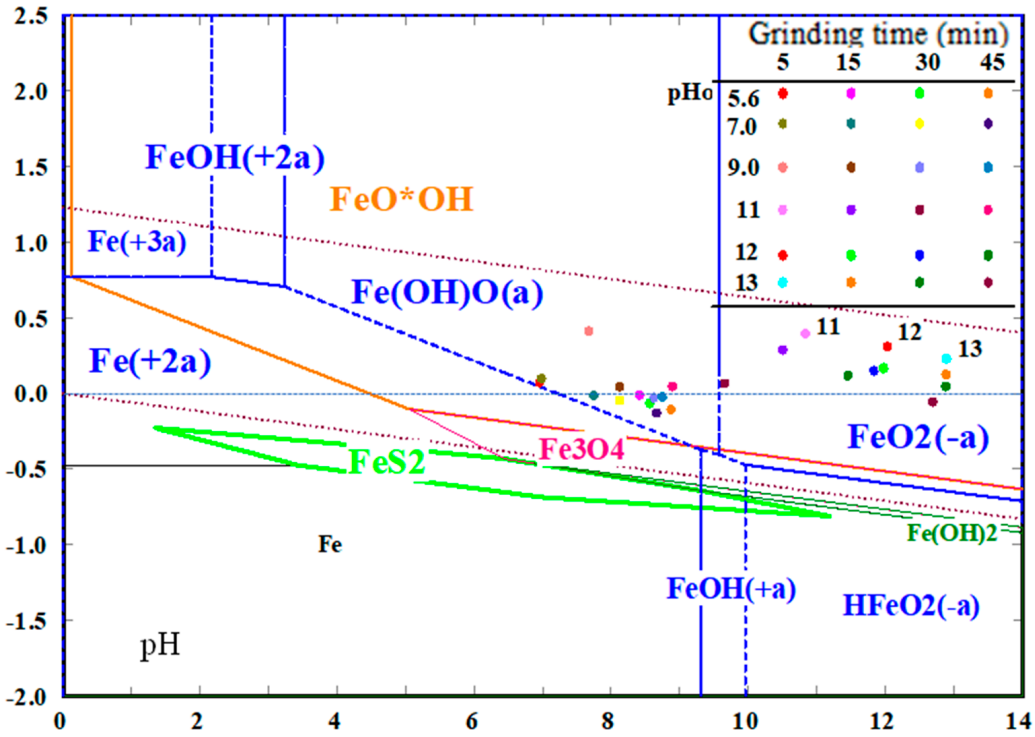

Figure 3. *Eh*—pH diagram of the Fe–S–H_2O system at 25 °C and 1M. Recorded pulp potential values and pulp potential values vs. standard hydrogen electrode.

Previous research studies have reported that the ions that determine the potential are a function of the ions in the solution (H^+, OH^-, Fe^{+2} and S^{2-}); therefore, the charge potential is governed by pH, pS and pFe [24]. The experimental results of the present study indicate that the concentrations of the sulphur and iron ions in the solution increased significantly during grinding, thus having a decisive influence on the properties of the pulp potential and on the superficial nature of the pyrite particles during the grinding tests.

The ICP analysis of these tests conducted only with grinding media and water at different pH values indicates that practically all of the iron resulting from the oxidation of the grinding media precipitated as an oxyhydroxide species. It should be noted that after each grinding test, the mill and the grinding media were thoroughly washed with concentrated sodium hydroxide, tap and distilled water, and dried with absorbent paper and air.

3.2. Surface Characterisation of Pyrite Obtained during Grinding

The solid particles of the pyrite obtained at each grinding time interval and for all the pH values were characterised by XRD, zeta potential, FTIR and SEM-EDS. Some of the samples were analysed for magnetic susceptibility using a magnetic susceptibility meter. In the XRD analysis for all of the tests, pyrite was detected as the main crystal species, identified with the diffraction pattern (DFP) 071-4755 of the JCPDS (Figure 4).

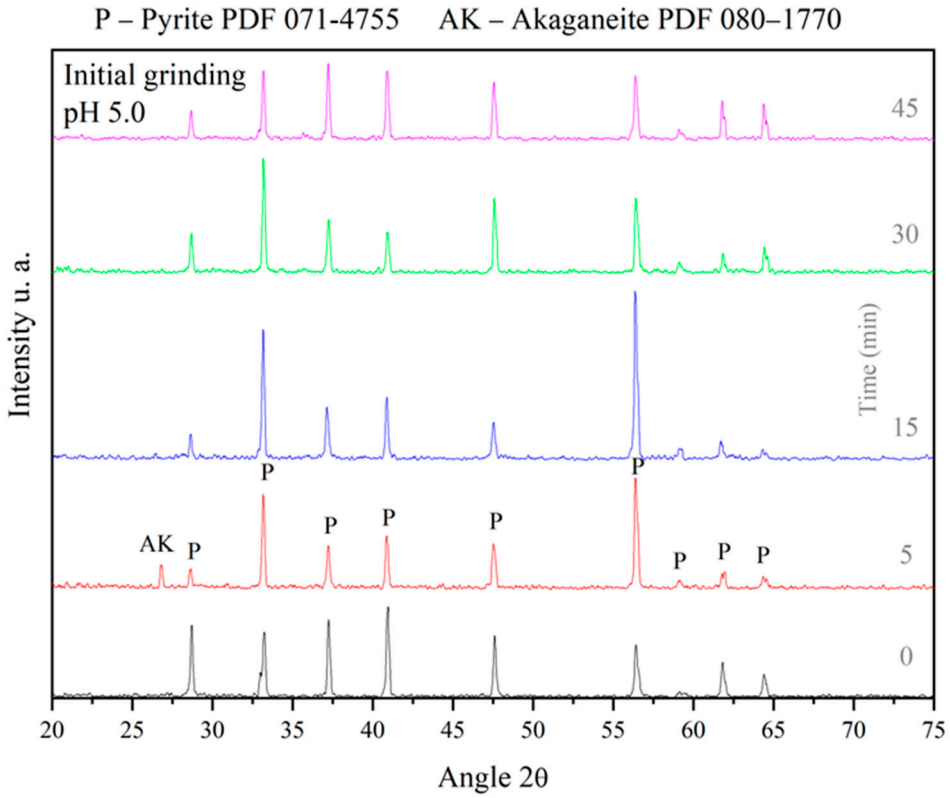

Figure 4. X-ray diffraction patterns of nonoxidised and oxidised pyrite obtained from grinding at an initial pH 5.0 and grinding times from 5 to 45 min.

Only at an initial pH of 5.0 and a 5 min grinding did the X-ray diffraction pattern present a peak different from that of pyrite, at 2θ 26.81, δ = 3.32 Å, which corresponded to the solid species akaganeite β-FeOOH, identified with the diffraction pattern (DFP) 080-1770 (Figure 4).

3.3. Zeta Potential (ζ; mV) and FTIR Spectroscopy of Pyrite Obtained during Grinding

The measurement of the zeta potential (ζ; mV) has been established as a diagnostic tool to determine the condition of the surface of a mineral [25]. It is defined as the decrease in the potential in the double layer that covers a charged particle between the slipping plane and the bulk solution [26]. The zeta potential allows to specifically determine the magnitude, apparent charge and the isoelectric point (IEP) or point of zero charge (PZC) of the particles of the pulp [26].

Figure 5 illustrates the behaviour of the zeta potential of the pyrite particles obtained during grinding with steel media for the different pH values and grinding times assessed. As the grinding time passed, changes occurred both in the pH and ζ. Overall, the measured values did not surpass +5 mV and kept a positive charge. The IEP values of the pyrite at pH < 3 in anaerobic conditions have previously been reported [27,28]. In other studies, the isoelectric point of the pyrite was detected at pH 7, due to the conversion of the ferrous iron of the pyrite into iron oxyhydroxides caused by the surface oxidation of the mineral particles [15].

In the present work, the reversal of the charge of the ζ occurred in some cases, for instance, at initial pH values of 5, 11 and 12 and grinding intervals of 30, 15 and 30 min, where the isoelectric point was determined at pH 8.5, 9.0 and 12.8, respectively. These values differ from those reported in the literature mainly because of the adsorption or formation of metal oxides, hydroxides and other species on the surface of the pyrite particle, which explains the ζ variation. It has previously been established that these measurements

do not represent pyrite, but they do represent the metal hydroxide species that cover the surface [29].

An increase in the formation and adsorption of the metal hydroxides on the surface of the pyrite results in a change in the magnitude and zeta potential, as reported in [28]. As mentioned above, the value of the ζ is correlated to the charge of the species that covers the surface of pyrite at a given pH, and it is influenced by the activity of the aqueous or ionic species in the solution [28]. However, the formation and adsorption of magnetite on the surface of pyrite has not yet been established. Our study provides evidence for the presence of magnetite on the surface of pyrite.

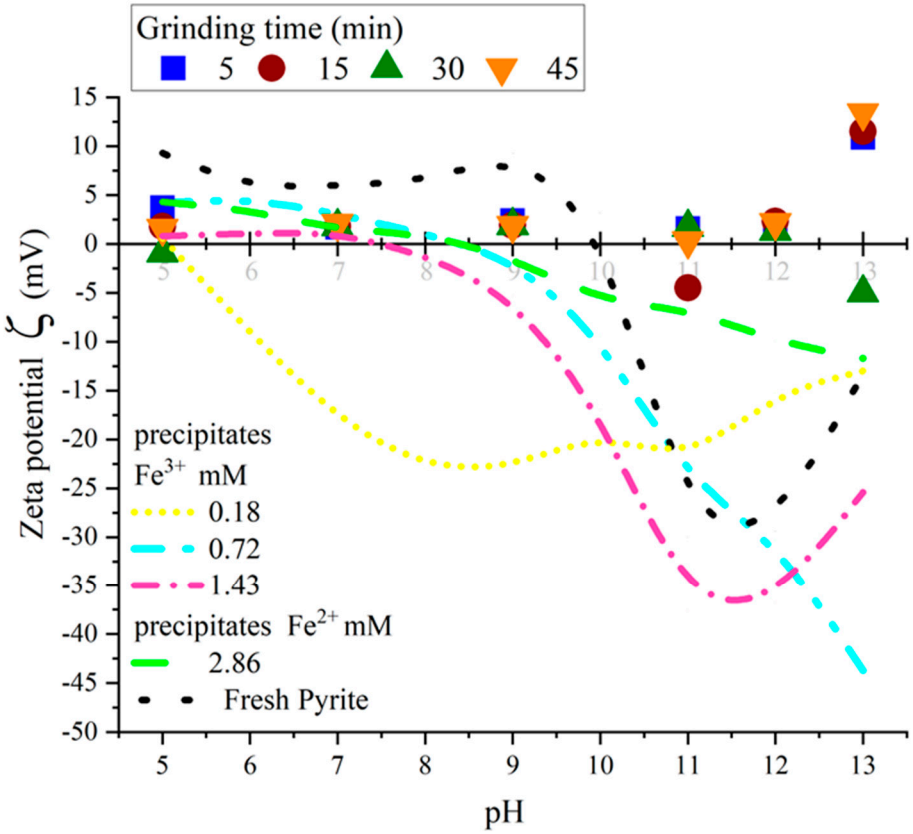

Figure 5. Zeta potential (ζ: mV) against pH of pyrite obtained from grinding and fresh grinding and of ferric (0.18, 072 and 1.43 mM) and ferrous iron precipitates (2.86 mM).

To determine the ζ of the pyrite particles freshly ground in an agate mortar and of the ferric and ferrous iron precipitates, independent experiments were conducted in a wide pH range (2–13). The aim was to determine their electrokinetic behaviour in relation to the ζ values of the pyrite obtained during grinding as well as to determine the attraction or repulsion of the precipitates into its surface and characterize the precipitated species by XRD and FTIR.

The zeta potential of the freshly ground pyrite studied in this work exhibited two isoelectric points (IEPs): one at pH 4.14 (not shown in Figure 5) and a second one at pH 10. The latter (zero charge pH) can be attributed to the presence of oxides and hydroxides on the surface of the pyrite. As can be seen in Figure 5, both the freshly ground pyrite particles and those obtained during grinding maintained a positive ζ in the initial pH zone 5–9 despite the difference in the surface speciation.

On the other hand, at the initial pH range 11–13, the pyrite obtained during grinding presented a zeta potential that contrasted with that of freshly ground particles. This was attributed to the differences in the ionic nature around the pyrite particles obtained during grinding and to their surface state of oxidation. In this case, in addition to the significant

amount of OH^- and Na^+ ions from NaOH, used to reach the desired pH values of 11, 12 and 13, we found a significantly high concentration of iron ions, which had the most stable phase at this pH range, and the *Eh* was FeO_2 (−a) and the sulphur ions were sulphate SO_4 (−2a). As highlighted in Figure 2a,b, these were aqueous species, which, along with the surface nature of the particles, have a decisive influence on the values and magnitude of the zeta potential.

Regarding the change in the polarity and magnitude of the ζ for the pyrite shown in Figure 5, it was correlated to the presence of a variety of secondary phases on the surface. In the literature, this reversal of the ζ was attributed to the adsorption of products from iron hydrolysis [30]. Figure 6 shows the FTIR spectra of the pyrite obtained during grinding with steel media at an initial pH of 5.0 and time intervals ranging from 5 to 45 min. A variety of species can be observed, which can directly affect the ζ values.

The broad and intense adsorption band at 605 cm^{-1} was attributed to the Fe–O bonds of the magnetite, which was identified in the infrared spectra of the ferrous iron Fe (+2) precipitates. The IR spectrum of the pyrite ground for 30 min, which showed a reversal from a positive to negative value of the ζ, had a distinctive presence of four absorption bands in the spectral zone of sulphur, at 1014, 1087, 1131 and 1192 cm^{-1}.

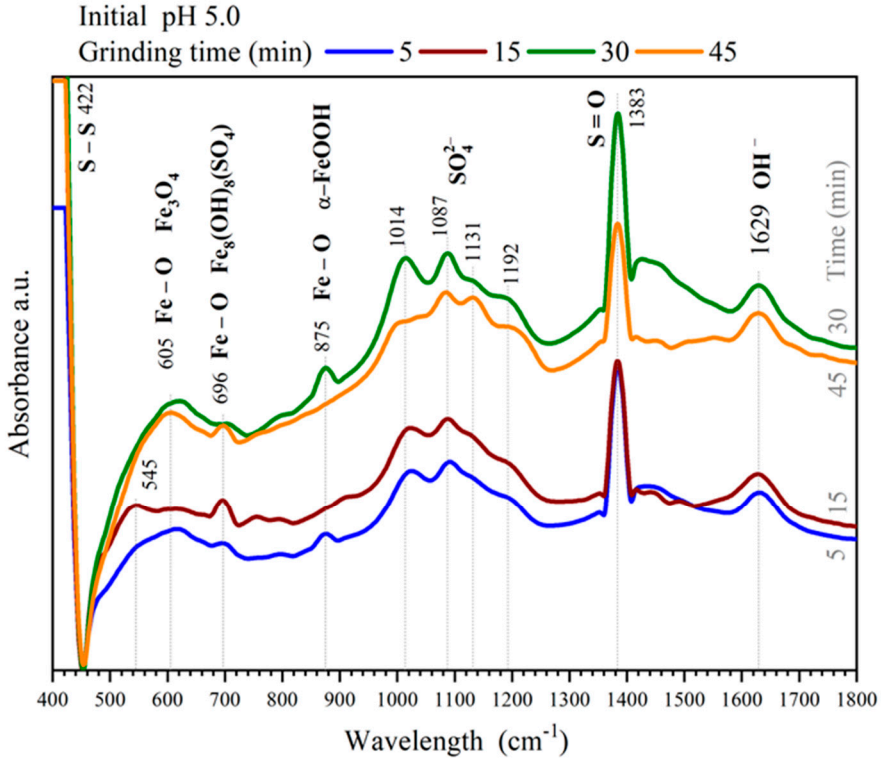

Figure 6. FT−IR spectra of pyrite ground with steel media at an initial pH of 5.0.

This is caused by the triply degenerate asymmetric stretching vibration ν_3 in the S–O bond. This indicates a bidentate coordination of iron with the sulphate ion on the pyrite surface; similar results have been reported [19]. Some researchers have found these absorption bands in oxidised minerals of iron, such as hematite [31].

The absorption band at 696 cm^{-1} indicates the vibration mode of the Fe–O bonds of iron hydroxysulfate $Fe_8(OH)_8(SO_4)$, which has been reported previously [18,20]. Such band was absent in the spectrum of the pyrite ground for 30 min; in addition, the decrease in this band favoured the growth of the signal detected at 1383 cm^{-1}, which was attributed to the vibration mode of the S=O bonds [32]. At 875 cm^{-1}, a relatively strong absorption band appeared, assigned to the stretching vibration of the Fe–O bonds of the goethite α-FeOOH. This species was not detected in the IR of the pyrite ground for 15 and 45 min; the species

described, together with the oxidised phases of the iron, led to the reversal of the polarity of the zeta potential.

The identification of the absorption band for the goethite was corroborated by the XRD and FTIR characterisation of the ferric iron solids that formed during the precipitation tests of the Fe (+3) ion at different concentrations.

The IR spectra of the pyrite obtained during grinding with steel media at an initial pH of 7.0 are shown in Figure 7. At 598 cm^{-1}, a relatively intense and broad band can be observed in all of the spectra; it corresponded to the Fe–O bonds of the magnetite Fe_3O_4. The weak signals located at 693 and 871 cm^{-1} corresponded to the formation of iron hydroxy sulphate $Fe_8O_8(OH)_6SO_4$ and goethite α-FeOOH, respectively. These absorption bands have been previously identified [15].

The main band of the sulphate ion, located at approximately 1200 cm^{-1}, split into four signals at 1036, 1084, 1130 and 1200 cm^{-1}, indicating a bidentate coordination between the sulphate and iron. The presence of sulfoxides can also be seen at 1384 cm^{-1}. Accordingly, the zeta potential of the pyrite particles obtained during grinding with an initial pH 7 had positive values.

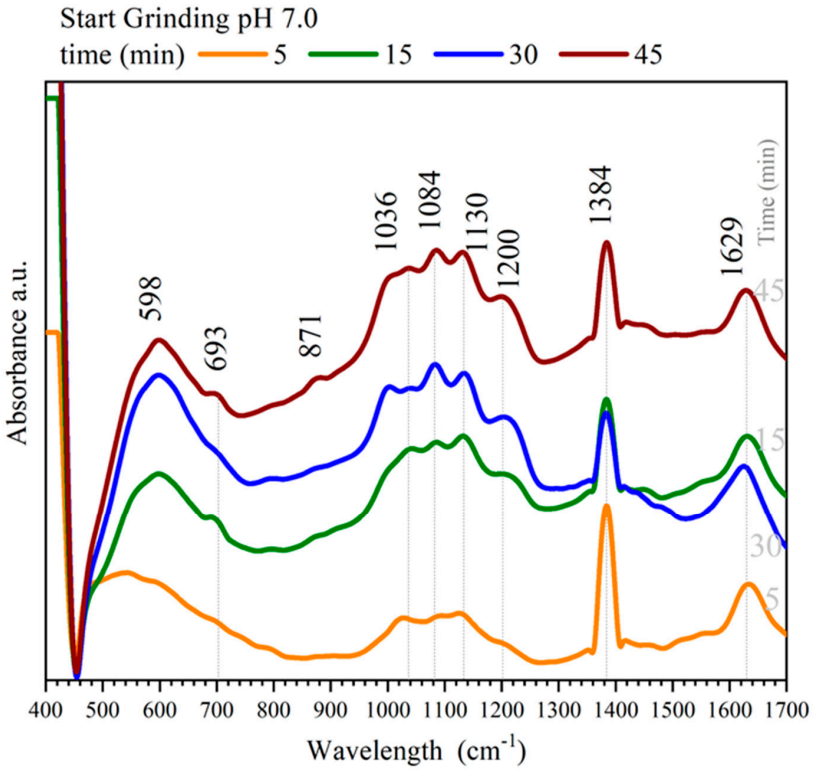

Figure 7. FT−IR spectra of pyrite ground with steel media (initial pH 7.0).

The pyrite particles obtained from grinding at pH 11, particularly those obtained after 15 min, showed polarity reversal of the zeta potential (ζ; mV), as detailed in Figure 8. This change was closely related to the presence of secondary phases detected on the surface of the pyrite and showed the IR spectra of the pyrite obtained after 5 min of grinding. The presence of carbonate-type species on the surface of the pyrite can be observed at the absorption band at 756 cm^{-1}; it corresponded to the stretching vibration of Fe–CO_3 (−2a), and it involved the coordination of the carbonate with the iron in compounds such as siderite, as mentioned above [19].

In addition, the bands at 1448 and 1493 cm^{-1} were attributed to the presence of the carbonate ions on the oxidised surface of the pyrite. These bands corresponded to the C–O symmetric and asymmetric stretching vibration modes, which were like those of bicarbonate HCO_3 (−a) or carboxylate ions but different from a typical carbonate molecule,

with only one absorption band at 1430 cm^{-1} [17]. The width of these bands indicated the presence of a carboxylate bidentate complex on the surface of the pyrite [15,19,20].

The presence of this carbonate-type species was attributed, on the one hand, to the pH and pulp conditions and, on the other, to carbon from the oxidation of the grinding media; in this case, not only iron but also carbon was released into the pulp solution. It is worth mentioning that the grinding media were made of carbon steel, and this gives rise to the formation of carbonate ions and Fe–CO_3 (−2a)-type bonds, which were detected through the spectra in Figure 8; these species have a decisive influence on the reversal of the zeta potential.

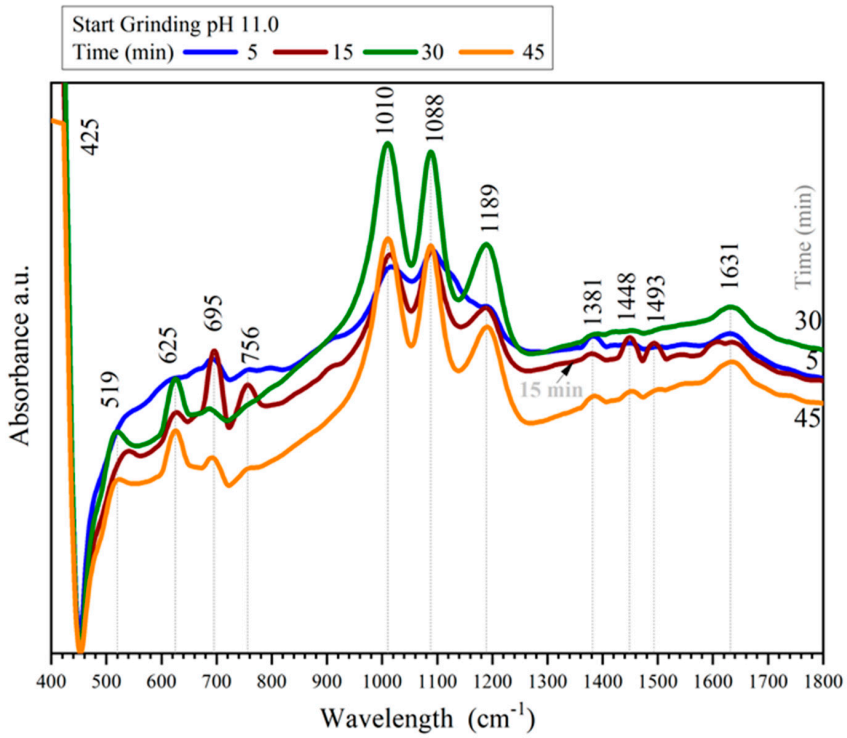

Figure 8. FT−IR spectra of pyrite ground with steel media (initial pH 11.0).

The main spectral zone of the sulphate ion split into three absorption bands: 1010, 1088 and 1189 cm^{-1}, indicating the formation of a monodentate compound between the bound sulphate and iron, as reported in [20]. The peaks at 519, 625 and 695 cm^{-1} corresponded to the Fe–O bonds of magnetite Fe_3O_4. In addition, a weak signal at 1381 cm^{-1} was assigned to the S=O bonds of sulfoxides.

It was observed that the pyrite particles obtained during grinding with steel media in all of the studied pH ranges and intervals showed magnetic attraction; therefore, magnetic susceptibility (K) measurements were carried out, using an MS2 Bartington Instruments magnetic susceptibility meter. The volumetric magnetic susceptibility and the specific magnetic susceptibility were calculated from Equations (2) and (3), respectively. In these equations [33], the VD factor is the measured value.

$$K = \frac{VD \times 10}{\text{Sample volume}}, \left[10^{-5}\, SI\right] \quad (2)$$

$$\chi = \frac{VD \times 10}{\text{sample weight}}, \left[10^{-8}\, m^3 kg^{-1}\right] \quad (3)$$

Figure 9 shows the specific magnetic susceptibility values $\chi\ 10^{-8}\ m^3\ Kg^{-1}$ of the pyrite particles obtained during grinding at pH 5 and 13 and at grinding times from 15 to 45 min. It can be appreciated that the pyrite particles ground in the agate mortar showed a χ of

practically zero, while the pyrite particles obtained during grinding at an initial pH of 7 had the highest specific magnetic susceptibility. The χ values decreased as the pH and grinding time increased.

However, they remained high, and only at pH 12 did the magnetic susceptibility decrease significantly, as illustrated in Figure 9. This characteristic of the surface of the pyrite particles obtained after grinding with steel media was attributed to the high degree of adsorption of the corrosion products and to the wear exerted by the grinding media and steel mill. It is worth recalling that the main species in these solids was magnetite Fe_3O_4.

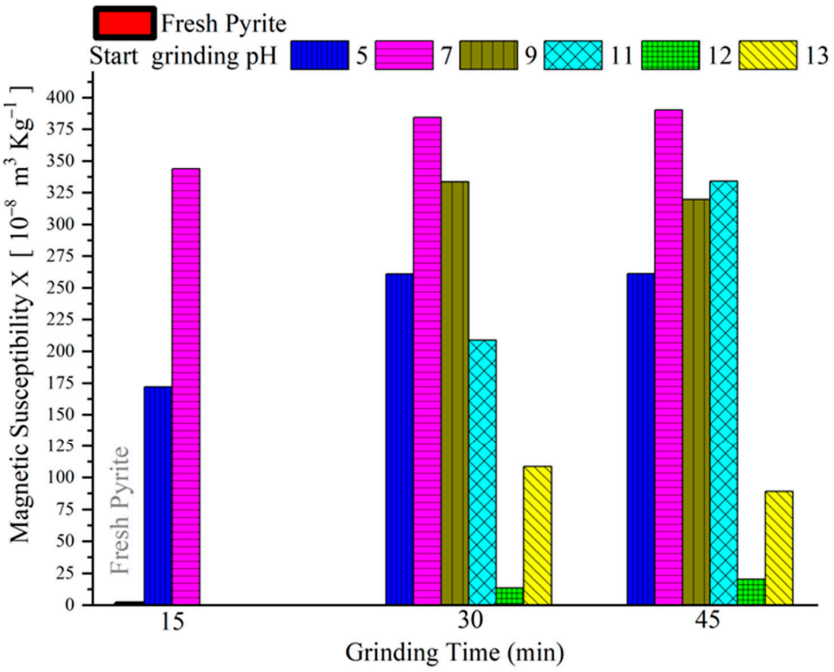

Figure 9. Specific magnetic susceptibility χ 10^{-8} m^3 Kg^{-1} of the pyrite particles obtained from grinding with steel media.

3.4. SEM-EDS Surface Characterisation of Pyrite Obtained during Grinding

The pyrite particles obtained from grinding at pH 5, 7 and 9 were analysed by scanning electron microscopy with energy-dispersive spectroscopy (Figure 10). They showed an elongated morphology with flat surfaces and sharp outlines. The conchoidal fracture was typical of pyrite. The microanalysis sites tagged as point 1 corresponded to a pyrite surface free of adsorbed particles or particles grown on the matrix, while the sites tagged as point 2 indicate the oxidised products of iron on its surface. In some cases, a point 3 was present, which corresponded to electrostatically attracted pyrite microparticles.

The micrographs in Figure 10A illustrate the particles obtained from grinding at an initial pH of 5 and grinding times of 5 and 30 min (left and right, respectively). The microanalyses corresponding to these micrographs indicate that an increase in the grinding time caused the oxygen and sulphur on pyrite surface point 1 to decrease, while the % of the iron increased, i.e., there was a surface rich in iron and poor in sulphur. As detailed above, at an initial pH of 5 and at 30 min of grinding, the zeta potential (ζ; mV) underwent a reversal of polarity.

Point 2 in the micrographs represents the species detected by FTIR, such as oxides, hydroxides and iron sulphates. It was found that as the grinding time increased, the oxygen concentration rose in the microparticles adsorbed onto the pyrite surface, while the iron decreased in the precipitate, and sulphur had no significant changes.

The micrographs of the pyrite particles obtained from grinding at an initial of pH 7 and at grinding times of 15 (left) and 45 (right) minutes are shown in Figure 10B. The pyrite surface that was macroscopically free of iron oxidation products showed an in-

crease in the oxygen concentration as the time advanced, while both sulphur and iron decreased proportionally.

As to the precipitates highlighted on point 2, they increased their oxygen concentration as the grinding progressed, while the sulphur and iron decreased (Figure 10B). The micrographs in Figure 10C present the pyrite particles obtained from grinding with steel media at an initial pH of 9 and reaction times of 5 and 45 min (left and right, respectively). The matrix surface that was free of iron precipitates did not show any considerable changes in correlation to the grinding time. However, the oxygen concentration was notably higher compared to the grinding pH values of 5 and 7, while iron and sulphur had percentages of approximately 35 % *w*/*w*.

Point 2 in the micrograph on the right, which corresponds to a reaction time of 45 min, indicated pyrite microparticles electrostatically attracted to the matrix surface, while point 3 corresponds to the semiquantitative analysis of the iron precipitates adsorbed onto the mineral surface. The iron precipitates present on the surface of the mineral not only decreased their sulphur and iron concentrations as the time increased, but they also lost oxygen.

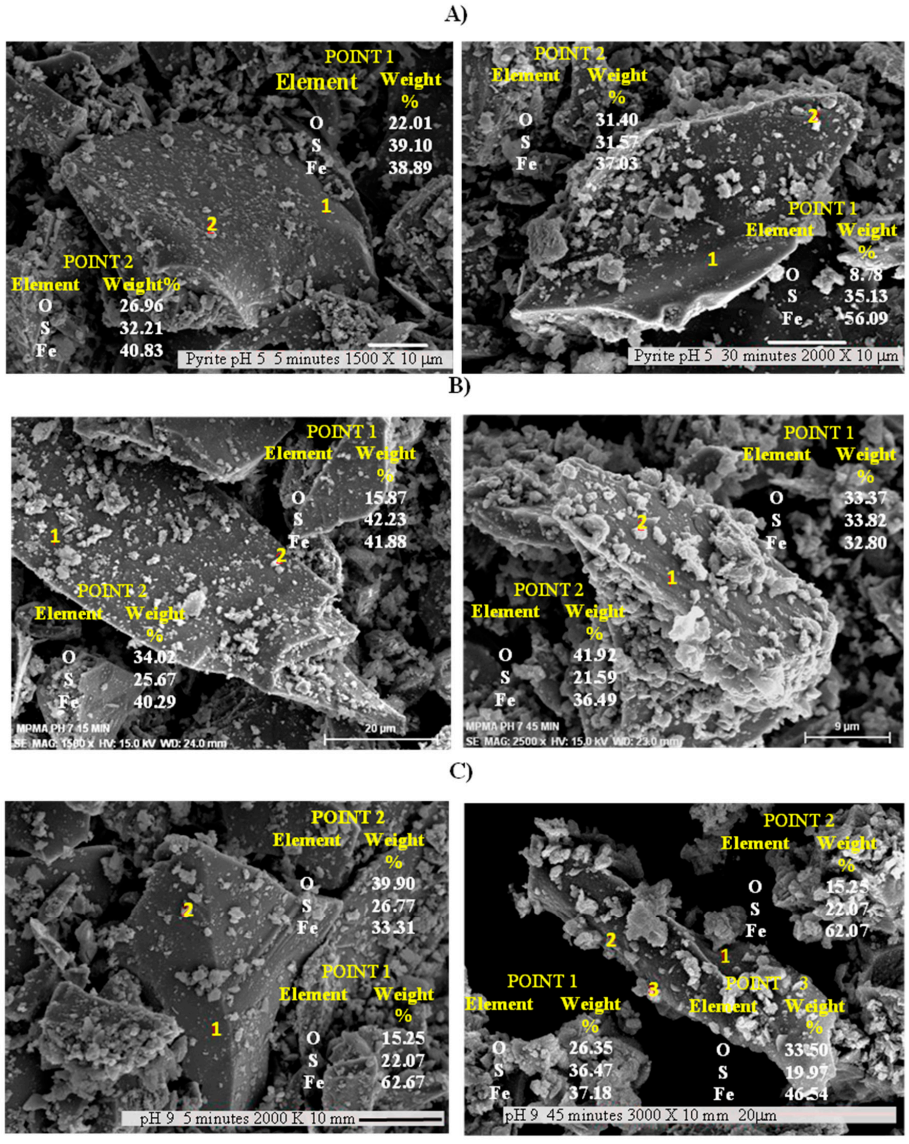

Figure 10. SEM-EDS micrographs of the pyrite particles obtained after grinding with steel media: initial pH 5 (**A**), 7 (**B**) and 9 (**C**).

3.5. FTIR Characterisation of Ferric and Ferrous Iron Precipitates

The behaviour of the zeta potential of the precipitates from solutions containing 0.18 mM Fe (+3) (Figure 5) exhibited the isoelectric point (IEP) at pH 5.0. At more acidic pH values, a positive ζ can be noted, while at pH values above the IEP, the ζ was negative. The iron precipitates at this concentration were electrostatically repulsive to the surface of the pyrite particles. Similar situations have been reported in the literature [13]. Also shown in Figure 5, the IEP for the precipitates from the 0.72 mM Fe (+3) solution was at pH = 8.3. Below the isoelectric point, the precipitates had a positive apparent surface charge, resembling the values of the pyrite particles ground in the steel mill at an initial pH range between 5 and 7. At pH values above IEP, the precipitates possessed an opposite charge to that of the pyrite particles ground at pH range 9–13, which led to the attraction of the iron precipitates onto the pyrite particles obtained during the grinding process.

In the synthetic ferric sulphate precipitation tests, the precipitates from solutions of 0.09, 0.18, 0.36, 0.72, 1.43 and 2.86 mM ferric iron (+3) showed a point of zero charge at pH values of 7.0, 5.0, 5.2, 8.3, 7.5 and 3.0, respectively. These changes are influenced both by the ionic nature surrounding the particles and the surface speciation of the ferric hydroxide precipitates, according to the FTIR characterisation.

Regarding the ferrous iron precipitates obtained from the 2.86 mM Fe (+2) solutions, these showed a zeta potential curve similar to the corresponding ferric hydroxyl precipitates at this same concentration. The isoelectric point of the Fe (+2) precipitates was found at pH 8.3. At pH above IEP, it was found that the negative values of the ζ kept rising due to the increase in the thickness of the double layer. This was caused by the excess of ions and counterions (Na^+, OH^-) surrounding the surface of the solid, thus producing a higher zeta potential.

The ferrous and ferric iron precipitates obtained at each pH value were characterised by XRD. As can be seen in Figure 11a, the diffraction patterns of the Fe (+2) corresponded, but only for the precipitates formed at pH 9, to a single polycrystalline phase, identified as magnetite, fcc Fe_3O_4, according to the 011–0614 JCPDS file, and were thermodynamically stable throughout the studied pH range. The XRD spectrum for the pH 5.0 precipitates indicated a low crystallinity powder, with some relatively wide, low-intensity peaks. As for the precipitates formed at pH 9, a second crystal phase was present, which was identified as lepidocrocite γ-FeOOH (JCPDS 008-0098).

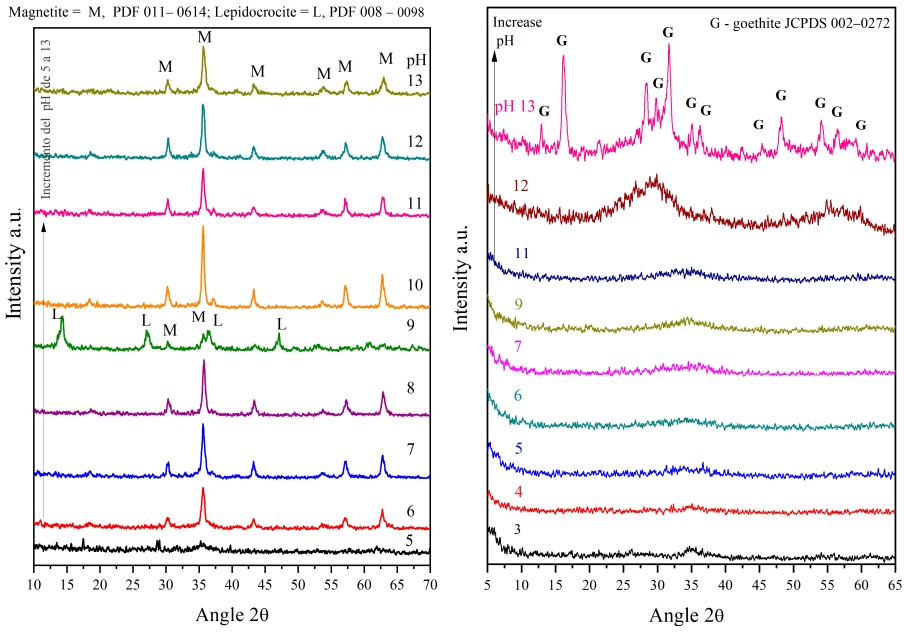

Figure 11. (**a**) Diffractograms of ferrous (+2) iron precipitates (2.86 mM concentration); (**b**) ferric (+3) iron precipitates (1.43 mM).

Figure 11b details the diffraction patterns of the iron (+3) hydroxides obtained from the solutions containing 1.43 mM Fe (+3) and 4.79 mM H_2SO_4. The crystal phase goethite, α-FeOOH, was identified (JCPDS 002–0272) only at pH 13. Below this pH value, the XRD patterns were essentially continuous in appearance, corresponding to noncrystalline materials. The α-FeOOH phase was also identified in the precipitates from the 2.86 mM Fe (+3) solutions.

The FTIR spectra of the solids precipitated from the 1.43 mM Fe (+3) solutions are shown in Figure 12. The absorption bands at 797 and 887 cm^{-1} were assigned to the Fe–O bond of α-FeOOH; both bands were distinctive of the iron precipitates obtained at pH 13, in agreement with the XRD results. The presence of this phase decreased the negative character of the zeta potential in the ferric ion precipitates.

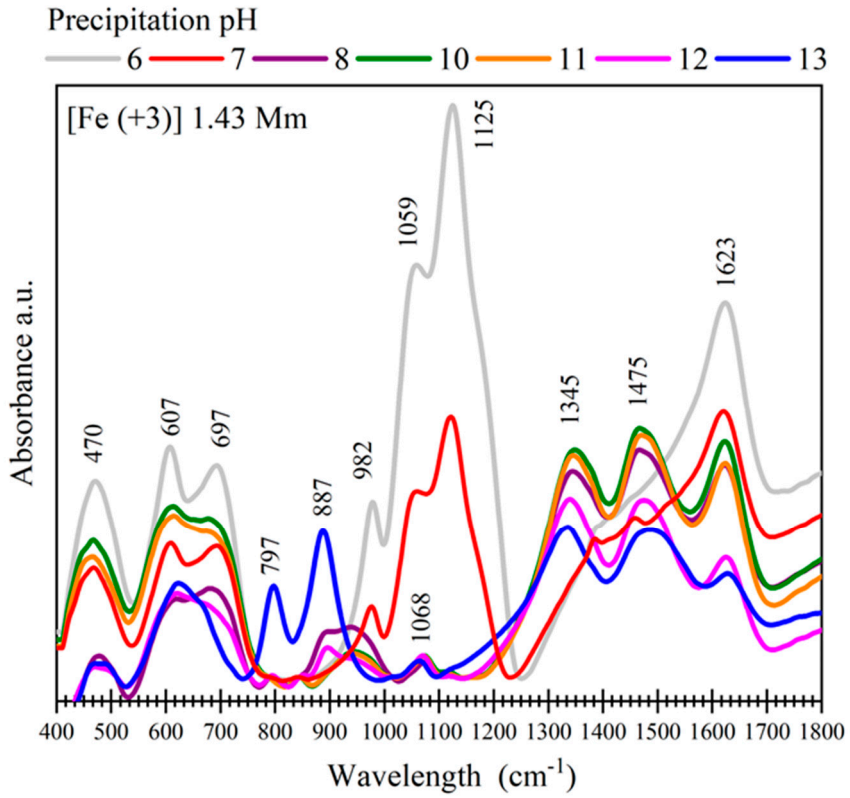

Figure 12. FT−IR spectra of the 1.43 mM Fe (+3) precipitates for the pH values 6, 7, 8, 10, 11, 12 and 13.

The spectral band at 470 cm^{-1} is present in all of the FTIR spectra in Figure 12. It corresponded to the iron oxyhydroxide identified as lepidocrocite, γ-FeOOH [18]. The absorption band at 607 cm^{-1} was attributed to akaganeite, β-FeOOH [32,34], and that appearing at 697 cm^{-1} corresponded to Schwertmannite, $Fe_8O_8(OH)_6SO_4$ [35]. The band at 1623 cm^{-1} represented the bending vibration of the water molecules adsorbed in the structure of the colloidal iron precipitate.

Moreover, in Figure 12, the spectral zone corresponding to sulphates (1000–1200 cm^{-1}) showed three absorption bands located at 982, 1059 and 1125 cm^{-1}, indicating the adsorption of the sulphate ion from the solution. The bands corresponded to the v_3 asymmetric stretching vibration of the sulphate ion [36]. The spectral profile was due to the low tetragonal symmetry of the SO_4^{2-} unit, resulting in the splitting of the v_3 band. These spectral changes have been dealt with in depth elsewhere [31,36,37]. The absence of the v_3 SO_4^{2-} triplet in the spectra corresponding to pH values above 7.0 was due to the decomposition of the sulphate at alkaline pH values [33]; therefore, the band appearing at 1068 cm^{-1} was not due to a SO_4^{2-} stretching vibration and could be assigned to the δ OH^- vibrational mode instead [37]. These changes in the particles of the precipitated iron hydroxides

were accompanied by a reversal of the zeta potential magnitude; its IEP was detected at pH = 7.5.

The identification of magnetite on the surface of the pyrite ground with steel media at approximately 620 cm^{-1} (Figure 13) was conducted through FTIR characterisation of the ferrous iron precipitates obtained from solutions containing 2.86 mM Fe (+2). The absorption band at 573 cm^{-1} and the weak absorption shoulders at 620 and 690 cm^{-1} were assigned to the Fe–O bonds of the magnetite.

The FTIR spectra of the precipitates obtained at pH 13 (Figure 13) showed absorption bands at 799 and 894 cm^{-1} corresponding to goethite, α-FeOOH, as found in the ferric iron precipitates under the same pH conditions. The formation of goethite caused the dissolution of the sulphates that were chemically coordinated with iron, which had absorption bands that appeared at 1016 and 1123 cm^{-1}.

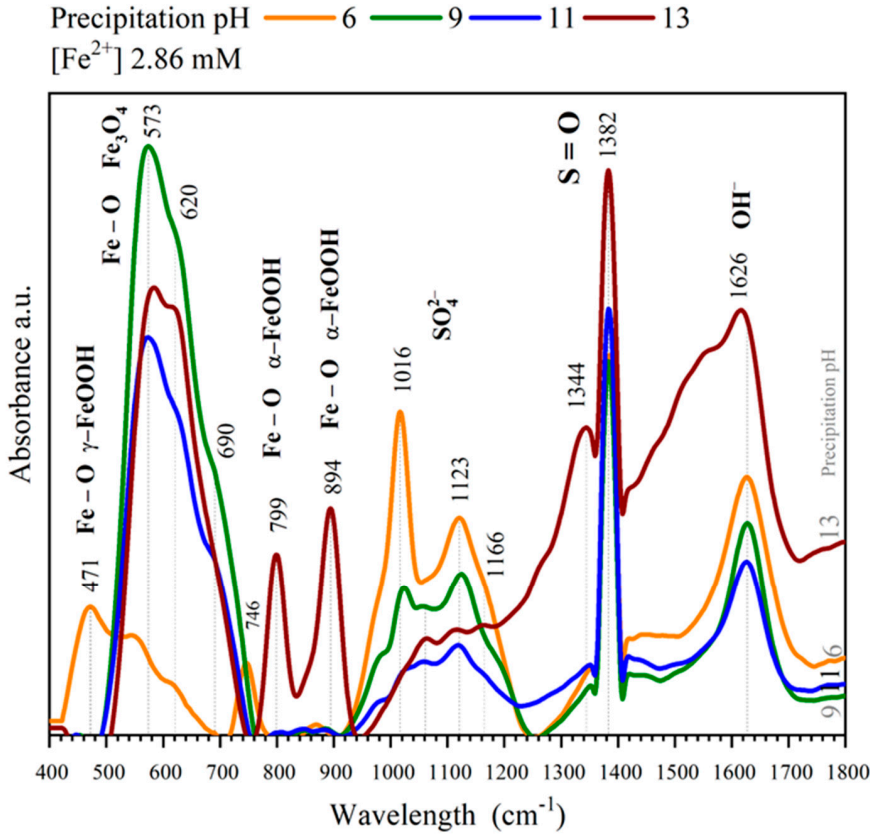

Figure 13. FT−IR spectra of the 2.86 mM Fe (+2) precipitates at pH = 6, 9, 11 and 13.

The intense peak appearing at 1382 cm^{-1} corresponded to the formation of sulfoxides S=O, formed by a reaction between chemisorbed oxygen and sulphur coprecipitated with magnetite. All of the FTIR spectra showed an absorption band at approximately 1626 cm^{-1}, assigned to the bending mode of the water molecules incorporated into the structure of the precipitates. The spectrum of the precipitates obtained at pH 6 showed a relatively strong band at 746 cm^{-1}, which was assigned to the Fe–O bonds in the Green Rust 2 complexes. Previous studies have reported that these complex species are magnetic phase precursors [38].

4. Conclusions

According to the results from the behaviour of the precipitates obtained at all pH ranges studied, the pyrite obtained during grinding with steel media showed magnetic susceptibility due to the presence of magnetite on the surface, which was identified by XRD and confirmed by the FTIR absorption band at approximately 598 cm^{-1}, corresponding to

the Fe–O bonds of Fe_3O_4. In addition, species, such as oxyhydroxy-sulphates and goethite, α-FeOOH, were identified at 696 and 875 cm^{-1}; these species cause the reversal of the zeta potential (ζ; mV) from positive to negative at pH 8.3 and 30 min of grinding. The ζ (mV) of the pyrite was positive (+5 mV); however, at pH 10.5 and 15 min of grinding, the ζ (mV) turned to negative values. This was associated with the formation of siderite Fe–CO_3 bonds, which were identified by the presence of FTIR absorption bands at 756, 1448 and 1493 cm^{-1}.

Author Contributions: Formal analysis, M.F.; Investigation, M.R., I.A.R., F.B. and G.H.; Methodology, F.P. and J.J.; Supervision, R.E. and E.G.P. All authors have read and agreed to the published version of the manuscript.

Funding: This research received no external funding.

Conflicts of Interest: The authors declare no conflict of interest.

References

1. Mu, Y.; Cheng, Y.; Peng, Y. The interaction of grinding media and collector in pyrite flotation at alkaline. *Miner. Eng.* **2020**, *152*, 106344. [CrossRef]
2. Hossein, M.; Mahdi, G. A review on electrochemical behavior of pyrite in the froth flotation process. *J. Ind. Eng. Chem.* **2017**, *47*, 1–18.
3. Rabieh, A.; Albijanic, B.; Eksteen, J.J. A review of the effects of grinding media and chemical conditions on the flotation of pyrite in refractory gold operations. *Miner. Eng.* **2016**, *94*, 21–28. [CrossRef]
4. Bicak, O.; Ekmekci, Z.; Bradshaw, D.J.; Harris, P.J. Adsorption of guar gum and CMC on pyrite. *Miner. Eng.* **2007**, *20*, 996–1002. [CrossRef]
5. Yelloji Rao, M.K.; Natarajan, K.A. Influence of galvanic interactions between chalcopyrite and some metallic materials on flotation. *Miner. Eng.* **1988**, *1*, 281–294.
6. Kant, C.; Rao, S.R.; Finch, J.A. Distribution of surface metal ions among the products of chalcopyrite flotation. *Miner. Eng.* **1994**, *7*, 905–916. [CrossRef]
7. Peng, Y.; Grano, S. Effect of grinding media on the activation of pyrite flotation. *Miner. Eng.* **2010**, *23*, 600–605. [CrossRef]
8. Adam, K.; Natarajan, K.A.; Iwasaki, I. Grinding media wear and its effect on the flotation of sulfide minerals. *Int. J. Miner. Process.* **1984**, *12*, 39–54.
9. Forssberg, E.; Subrahmanyam, T.V. Grinding, pulp chemistry and particle floatability. In *Proceedings of the XVIII International Mineral Processing Congress, Sydney*; The Australasian Institute of Mining and Metallurgy: Melbourne, Australian, 1993; Volume 1, pp. 1–6.
10. Fontana, M.G. *Corrosion Engineering*, 3rd ed.; McGraw-Hill International: New York, NY, USA, 1987.
11. Ralston, J. Eh and its consequences in sulphide mineral flotation. *Miner. Eng.* **1991**, *4*, 859–878. [CrossRef]
12. Leja, J. *Surface Chemistry of Froth Flotation*; Plenum Press: New York, NY, USA, 1982.
13. Peng, Y.; Grano, S. Inferring the distribution of iron oxidation species on mineral surfaces during grinding of base metal sulphides. *Electrochim. Acta* **2010**, *55*, 5470–5477. [CrossRef]
14. Peng, Y.; Grano, S.; Fornasiero, D.; Ralston, J. Control of grinding conditions in the flotation of galena and its separation from pyrite. *Int. J. Miner. Process.* **2003**, *70*, 67–82. [CrossRef]
15. Caldeira, C.L.; Ciminelli, V.S.T.; Dias, A.; Osseo Asare, K. Pyrite oxidation in alkaline solutions: Nature of the product layer. *Int. J. Miner. Process.* **2003**, *72*, 373–386.
16. Posey Dowty, J.; Moskowitz, B.; Crerar, D.; Hargraves, R.; Tanenbaum, L.; Dowty, E. Iron oxide and hydroxide precipitation from ferrous solutions and its relevance to Martian surface mineralogy. *Icarus* **1986**, *66*, 105–116. [CrossRef]
17. Cornell, R.M.; Schwertmann, U. *The Iron Oxides. Structure, Properties, Reactions, Occurrences and Uses*, 2nd ed.; Wiley—Vch: New York, NY, USA, 2003; Volume I.
18. Bigham, J.M.; Carlson, L.; Murad, E. Schwertmannite, a new iron oxyhydroxysulphate from Pyhäsalmi, Finland, and other localities. *Mineral. Mag.* **1994**, *58*, 641–648. [CrossRef]
19. Caldeira, C.L.; Ciminelli, V.S.T.; Osseo Asare, K. The role of carbonate ions in pyrite oxidation in aqueous systems. *Geochim. Et Cosmochim. Acta* **2010**, *74*, 1777–1789. [CrossRef]
20. Descostes, M.; Beaucaire, C.; Florence, M.; Savaoy, S.; Sow, J.; Zuddas, P. Effect of carbonate ions on pyrite (FeS_2) dissolution. *Bull. Société Géologique Fr.* **2002**, *173*, 265–270. [CrossRef]
21. Donato, P.; Mustin, C.; Benoit, R.; Erre, R. Spatial distribution of iron and sulphur species on the surface of pyrite. *Appl. Surf. Sci.* **1993**, *68*, 81–93.
22. Guy, P.J.; Trahar, W.J. The influence of grinding and flotation environments on the laboratory batch flotation of galena. *Int. J. Miner. Process.* **1984**, *12*, 15–38. [CrossRef]

23. Taylor, B.E.; Wheeler, M.C.; Nordstrom, D.K. Stable isotope geochemistry of acid mine drainage: Experimental oxidation of pyrite. *Geochim. Cosmochim. Acta* **1984**, *48*, 2669–2678. [CrossRef]
24. Weerasooriya, R.; Tobschall, H.J. Pyrite–water interactions: Effects of pH and pFe on surface charge. *Colloids Surf. A Physicochem. Eng. Asp.* **2005**, *264*, 68–74. [CrossRef]
25. Barnes, A.; Sapsford, D.J.; Dey, M.; Williams, K.P. Heterogeneous Fe (II) oxidation and zeta potential. *J. Geochem. Explor.* **2009**, *100*, 192–198. [CrossRef]
26. Stumm, W.; Morgan, J.J. *Aquatic Chemistry: Chemical Equilibria and Rates in Natural Systems*, 3rd ed.; John Willey and Sons: New York, NY, USA, 1996.
27. Erdemoglu, M.; Sarıkaya, M. Effects of heavy metals and oxalate on the zeta potential of magnetite. *J. Colloid Interface Sci.* **2006**, *300*, 795–804. [CrossRef] [PubMed]
28. Fornasiero, D.; Eijt, V.; Ralston, J. An electrokinetic study of pyrite oxidation. *Colloids Surf.* **1992**, *62*, 63–73. [CrossRef]
29. Healy, T.W.; Moignard, M.S. A review of electrokinetics studies of mineral sulfides. In *Flotation Gaudin, A.M. Memorial*; AIME: New York, NY, USA, 1976; pp. 275–291.
30. Fullston, D.; Fornasiero, D.; Ralston, J. Zeta potential study of the oxidation of copper sulfide minerals. *Colloids Surf. A Physicochem. Eng. Asp.* **1999**, *146*, 113–121.
31. Hug, S.J. In Situ Fourier Transform Infrared Measurements of Sulfate Adsorption on Hematite in Aqueous Solutions. *J. Colloid Interface Sci.* **1997**, *2*, 415–422.
32. Nakamoto, K. *Infrared and Raman Spectra of Inorganic and Coordination Compounds*, 3rd ed.; Wiley: New York, NY, USA, 1978.
33. Burgardt, P.; Seehra, M.S. Magnetic susceptibility of iron pyrite (FeS_2) between 4.2 and 620 K. *Solid State Commun.* **1977**, *22*, 153–156.
34. Reyes, I.A.; Mireles, I.; Patiño, F.; Pandiyan, T.; Flores, M.U.; Palacios, E.G.; Gutiérrez, E.J.; Reyes, M. A study on the dissolution rates of KCr (VI) jarosites: Kinetic analysis and implications. *Geochem. Trans.* **2016**, *17*, 3.
35. Chirita, P.; Descostes, M.; Schlegel, M.L. Oxidation of FeS by oxygen-bearing acidic solutions. *J. Colloid Interface Sci.* **2008**, *321*, 84–95.
36. Frost, R.; Wills, R.A.; Kloprogge, J.; Martens, W. Thermal decomposition of ammonium jarosite $(NH_4)Fe_3(SO_4)_2(OH)_6$. *J. Therm. Anal. Calorim.* **2006**, *84*, 489–496. [CrossRef]
37. Bishop, J.L.; Murad, E. The visible and infrared spectral properties of jarosite and alunite. *Am. Mineral.* **2005**, *90*, 1100–1107.
38. Cornell, R.M.; Schneider, W. Phase transformations in the ferrihydrite/cysteine system. *Polyhedron* **1989**, *8*, 2829–2836. [CrossRef]